

AUTOGENOUS HEALING OF FIBER/MATRIX INTERFACE AND ITS ENHANCEMENT

JISHEN QIU, SHAN HE, QIANG WANG, HAIBIN SU AND EN-HUA YANG

Nanyang Technological University
50 Nanyang Avenue, Singapore 639798

e-mail: jishen.qiu@colorado.edu

e-mail: heshan@ntu.edu.sg,

e-mail: wangqntu@gmail.com,

e-mail: ehyang@ntu.edu.sg

email: haibinsu@ust.hk

Key words: Autogenous healing; fiber/matrix interface; interface bond strength; polymeric fiber; hydraulic cement; fiber-bridging strength

Abstract: Fiber-reinforced cementitious composites (FRCC) represent a large group high-performance concrete for buildings and constructions. In this paper, the long ignored autogenous healing at debonded micro fiber/cement matrix interface ($\sim 1 \mu\text{m}$ crack) is demonstrated for the first time. Class F fly ash, a common Portland cement replacement that is rich in silicate, is engaged to promote interfacial healing. Single micro fiber pullout tests and microstructural characterization show that the presumed fiber/matrix healing indeed takes place and causes significant increase of the mechanical bond between fiber and matrix; additional silicate-rich fly ash greatly improves the healing efficiency. Uniaxial tensile test to the fiber-bridging indicates that the fiber/matrix interfacial healing can enhance the tensile strength of FRCC.

1 INTRODUCTION

Self-healing in cementitious composites is categorized into two groups: autonomic healing and autogenous healing. In autonomic healing, alien components such as carbonate-precipitating bacteria [1-2], microcapsules housing chemical agents [3], and vascular networks [4], are embedded in cement-based matrix; the healing agents are activated or released when hit by the propagating crack and exposed to ambient environment. By engaging significant amount of healing products, autonomic healing can seal crack width of $500 \mu\text{m}$ or larger [5]; however, it only delivers limited mechanical recovery and leaves the sealed crack as the weak spot to new mechanical loading. Autonomic healing is more suitable for non-structural surface cracks, which introduce aggressive agent and undermine the durability of reinforced

concrete.

Autogenous healing, on the other hand, relies on the residual chemical reactivity of the cement paste alone: in the presence of water, Ca^{2+} ions (rich in C-H and C-S-H) in cement paste are dissolved and leached out to crack space, where they encounter dissolved CO_2 (*i.e.*, CO_3^{2-}) and form CaCO_3 as healing products. However, it happens only when the crack width is controlled to be smaller than $50\text{-}100 \mu\text{m}$ (depending on the specific cement matrix composition) [6-7], which creates a local chemical environment that favors the precipitation of CaCO_3 . Autogenous healing is often observed in fiber-reinforced cementitious composites (FRCC), where the fiber-bridging is intentionally designed to realize fine crack width (*e.g.*, strain-hardening cementitious composites, SHCC) [7-9].

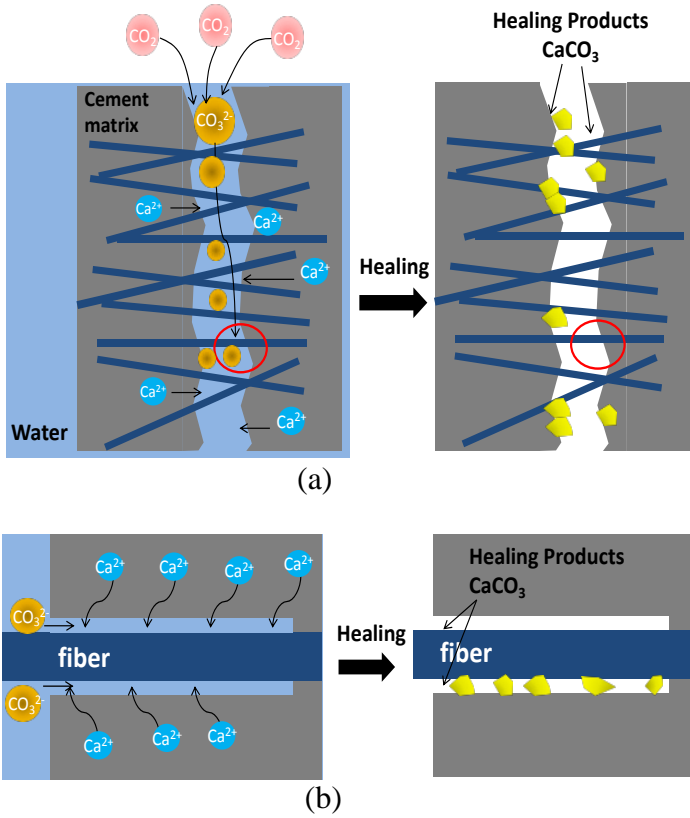


Figure 1: Autogenous healing in FRCC: (a) matrix crack; (b) fiber/matrix interfacial crack, its location is indicated by the red circles in (a)

Unlike conventional concrete, the cracking in FRCC happened on two scales: the matrix cracking exposes the fiber-bridging; after that the fibers are debonded by fiber/matrix interfacial cracking and pulled out from the matrix, leading to fiber-bridging loss and material failure. Fig. 1 illustrates the two-scale healing in FRCC: in matrix crack (Fig. 1a), healing products form and partially sealed the crack space, which is essentially no different from the autogenous healing in conventional concrete; assumably, in fiber/matrix interfacial crack (Fig. 1b), healing products would appear through similar chemical reaction. Recent studies have shown that the tensile performance FRCC recovered significantly even when the matrix crack is not fully closed by healing conditioning [7,9-10], further suggesting the existence of fiber/matrix interfacial healing. Intensive studies have been carried out to understand the matrix crack healing in FRCC and the consequent

improvement on FRCC durability; on the other hand, the fiber/matrix interfacial crack was rarely characterized in situ, and no study has been carried out to demonstrate the autogenous healing of the interfacial crack.

In the current study, fiber/matrix interface healing is examined for the first time. Experiments were carried out to evaluate the healing-induced recovery of fiber/matrix interface bond strength. Furthermore, effects of matrix compositions on the recovery of fiber/matrix interface bond strength and fiber-bridging capacity were investigated and reported. Scanning electron microscopy (SEM) and energy-dispersive X-ray (EDX) spectroscopy were engaged to characterize the morphology and chemical compositions of the healing products, respectively.

2 MATERIALS AND METHODS

2.1 Experiment to characterize interfacial healing

Long polyvinyl alcohol (PVA) fibers with circular cross section and an average diameter of $46 \pm 4 \mu\text{m}$ were used in the current study. Type I Portland cement (OPC) and class F coal fly ash (FA) were used to prepare the cement matrix. The chemical compositions of OPC and FA can be found in Table 1. A polycarboxylate-based superplasticizer (SP) was used to enhance the flowability of fresh paste mixture. Two mix proportions with different contents of fly ash (FA0 and FA35) were prepared to study the effects of matrix composition on interface healing. The specific mix proportions of FA0 and FA35 were PC : FA : W (water) : SP = 1.0 : 0.0 : 0.3 : 0.002 and PC : FA : W : SP = 0.65 : 0.35 : 0.3 : 0.002, respectively. The relative ratios are given in weight.

A single fiber embedded in cement matrix specimens, namely single fiber/matrix specimen, were prepared to examine the interfacial healing. Manufacturing of the specimens followed the procedures below: the cement, fly ash, and superplasticizer were premixed with water in a small kitchen mixer for five mins; the fresh mixture was then cast

into a plate mold with parallel long PVA fibers protruding out of the mold. The fresh mixture was kept in the ambient air ($25\pm 3^\circ\text{C}$) for 24 hours. The specimen was then demolded and kept in the same condition for over 50 days before cutting into thin specimens (1.2 ± 0.3 mm in thickness, i.e. embedment length) with a Buehler Isomet 1000 precision saw. More details on the specimen preparation can be found in [11].

Table 1: Example of the construction of one table

Component	Content (%)	
	OPC	FA
CaO	62.2	1.2
SiO ₂	24.3	58.6
Al ₂ O ₃	4.6	30.4
Fe ₂ O ₃	4.0	4.7
MgO	3.3	0.8
TiO ₂	0.6	2.0
K ₂ O	0.5	1.5
Na ₂ O	0.2	0.0
P ₂ O ₅	0.2	0.5
Others	0.1	0.3

The interfacial crack between fiber and matrix was induced by pulling the fiber with an MTS Acumen Model 1 Electrodynamic Test System, which equipped with a specially customized 10 N load cell (Fig. 2). The tensile loading was applied in displacement-control manner at 0.3 mm/min for both preloading and reloading. The pre-loading was immediately stopped once a sudden load drop was detected, which indicated the completion of fiber debonding [12], and the pre-loaded specimens were removed from the machine.

In order to engage autogenous healing, some of the pre-loaded specimens were conditioned under eight water/air cycles. Each cycle consisted of one day immersed in tap water ($25\pm 3^\circ\text{C}$) and one day in ambient air ($25\pm 3^\circ\text{C}$). The remaining pre-loaded specimens were only conditioned in the ambient air ($25\pm 3^\circ\text{C}$) for the same healing duration, i.e., 16 days. This is to investigate the effects of different conditioning regime on interface healing. Another group of specimens without any pre-loading was also conditioned for eight water/air cycles, as the control to

reveal any potential change of interface bond strength due to further hydration from the eight water/air conditioning cycles. After conditioning, all specimens were reloaded to evaluate the recovery of interface bond strength.

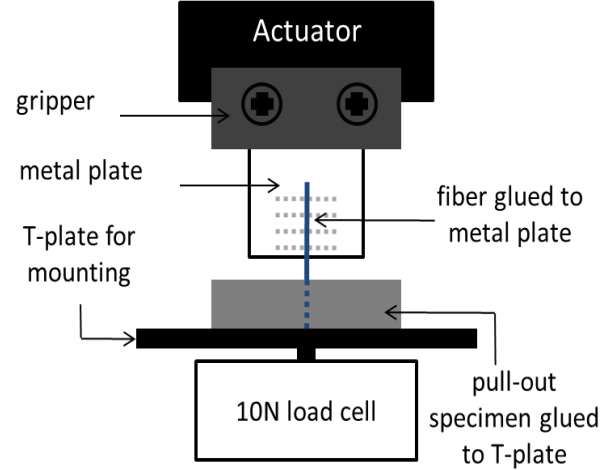


Figure 2: Single-fiber testing set-up to induce crack between fiber and matrix

2.2 In-situ characterization of fiber/matrix interface

The fiber/matrix interface was characterized in-situ under FE-SEM equipped with EDX (Fig. 3) before pre-loading, after-preloading, and after healing. The single fiber/matrix specimen was first impregnated by the Buehler Epothin hardener and resin at a ratio of 1:1.6 in a cylinder mold (Φ 30 mm, height 15 mm). After hardening in 24 h, the impregnated sample was demolded and carefully ground using P1200 sand paper to expose the bottom side of the single fiber/matrix specimen. The debris from grinding was removed in an ultrasonic cleaner for five mins. The grinding/cleaning procedure was repeated for several times. The exposed cross section was then polished on a Buehler MetaServ 250 platform equipped with a Vector polishing head for 15 min with 1 μm dissolved diamond paste applied to the polishing area. Immediately after polishing, the sample was ultrasonically cleaned for five minutes. The sample was then kept in a relatively dry environmental cabinet (23.6°C , 42% RH) until the FE-SEM/EDX characterization in the next day.

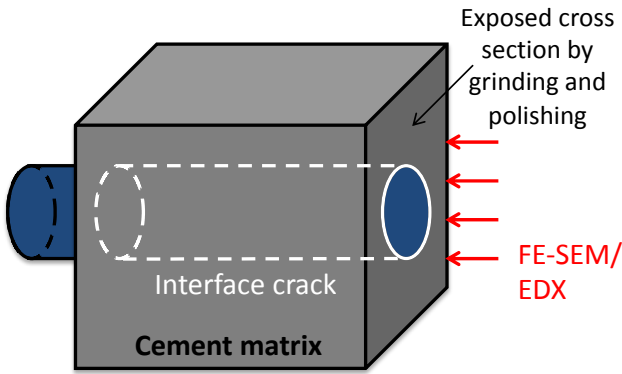


Figure 3: Illustration of the interface crack under FE-SEM/EDX characterization

2.3 Experiment to characterize the healing of fiber-bridging

The healed fiber/matrix interface shall have a direct impact on the recovery of fiber-bridging of FRCC. Uniaxial tensile tests were carried out to quantify the healing-induced recovery of fiber-bridging strength of FRCC. Both FA0 and FA35 were studied. The specific mix proportion of FA0 and FA35 were PC : FA : W : SP : fiber = 1.0 : 0.0 : 0.3 : 0.002 : 0.003 and PC : FA : W : SP : fiber = 0.65 : 0.35 : 0.3 : 0.002 : 0.003, respectively. The relative ratios are given in weight. All materials were the same as those used in Sec 2.1 except short 12 mm PVA fibers were used for the FRCC sample preparation.

The fresh FRCC materials were prepared in a 20L planetary mixer. All materials except fibers were mixed first for five minutes. After which, the fibers were added within two minutes and mixed until all fibers are well-dispersed in the matrix. The fresh FRCC mixture was cast into dog-bone molds (Fig. 5). The specimens were kept in the ambient air ($25\pm 3^\circ\text{C}$) for 24 h before demolding. The demolded specimens were then kept in the water ($25\pm 3^\circ\text{C}$) for 27 days before further tests.

The specimens were uniaxially pre-loaded at a loading rate of 0.2 mm/min using an Instron 5569 loading frame. On each specimen, only one matrix crack was generated during the pre-loading. Some pre-cracked specimens (seven for each mix design) were then conditioned for eight water/air cycles before reloading. Each conditioning

cycle consisted of one day immersed in tap water ($25\pm 3^\circ\text{C}$) and one day in ambient air ($25\pm 3^\circ\text{C}$). The remaining pre-cracked specimens (six for each mix) were conditioned in the ambient air ($25\pm 3^\circ\text{C}$) for the same duration, i.e., 16 days. This is again to investigate the effects of different conditioning regime on healing-induced fiber-bridging recovery. The surface crack width of each specimen was measured with a Nikon DS-Fi2 high resolution camera at magnification of 140 \times . Another group of FRCC specimens without any pre-cracking was also conditioned for eight water/air cycles as the control to reveal any potential change of fiber-bridging strength due to further hydration from the eight water/air conditioning cycles. After conditioning, the specimens were reloaded at the same loading rate with the same set-up to evaluate the recovery of fiber-bridging strength.

3 RESULTS AND DISCUSSIONS

3.1 Healing-induced recovery of interface bond strength

Fig. 4 shows the typical fiber pullout force vs. fiber displacement curves of single fiber/matrix specimen (FA0). A sudden load drop from P_a to P_b can be observed during the pre-loading, which indicated the completion of fiber/matrix interface debonding and loss of interface chemical bond between fiber and matrix [12]. For pre-loaded specimens conditioned in the ambient air (Fig. 4a), the reloading curve ramps linearly with a slope similar to the pre-loading curve and it soon returns to the point where the pre-loading had been stopped ($P_b' = P_b$). After that the curve enters into the fiber slippage stage. Since the interfacial friction is limited, the fiber can be entirely pulled out without rupturing. For the pre-loaded specimens conditioned in the water/air cycles (Fig. 4b), the reloading curve ramps with a slope steeper than the pre-loading curve, and enters into the slippage stage at a remarkably higher load $P_b' > P_b$. The interface friction keeps increasing due to the slip-hardening effect [12] resulting in fiber

rupture. However, the pullout force of the reloading curve in Fig. 6b is still significantly lower than that of the control group (Fig. 4c), which indicates the interface bond strength was not fully recovered. It is noteworthy that no sudden load drop is observed in the reloading curve, which suggests that water/air conditioning did not re-establish the interface chemical bond between fiber and matrix.

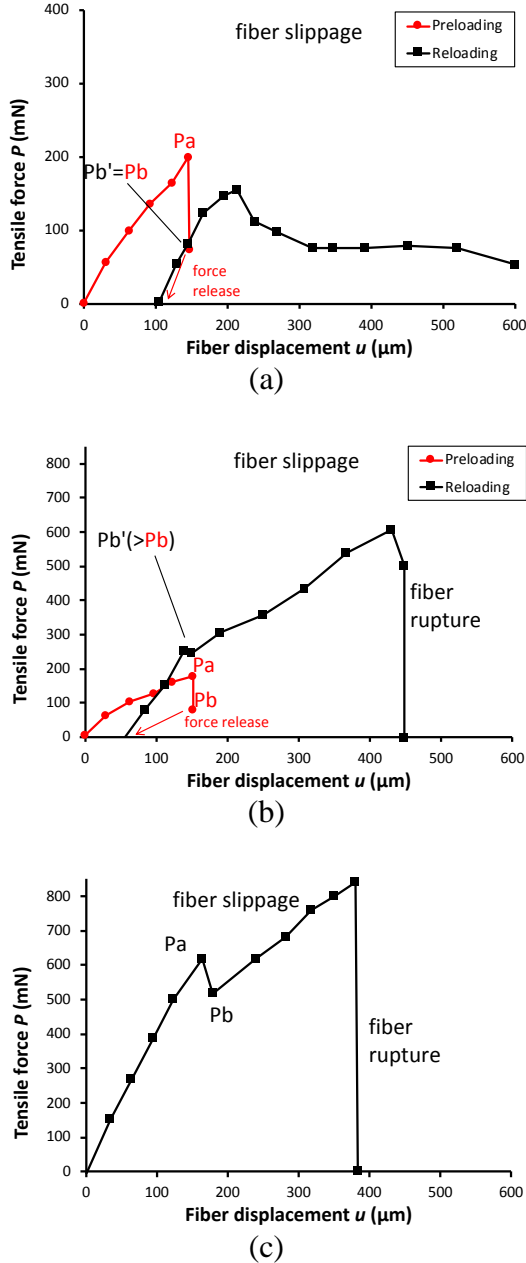


Figure 4: Fiber pullout force vs. fiber displacement curves of single fiber/matrix specimen (FA0): (a) Pre-loaded specimen with air conditioning; (b) pre-loaded specimen with water/air conditioning; (c) control specimen under water/air conditioning.

3.2 Interface healing enhancement by FA

The interface frictional bond strength can be derived from the pullout force vs. fiber displacement curves in accordance with [12] as follows,

$$\tau_0 \text{ (or } \tau) = P_b \text{ (or } P_b') / (\pi d_f L_e) \quad (1)$$

where τ_0 is the original interface frictional bond strength before healing, which can be derived from the pre-loading curves in Figs. 4a and 4b; τ is the interface frictional bond strength of pre-loaded specimen after conditioning, which can be derived from the reloading curves in Figs. 6a and 6b; d_f is the fiber diameter; and L_e is the fiber embedment length. The healing degree η is defined by Eq. 2 as follows,

$$\eta = \tau / \tau_{control} \quad (2)$$

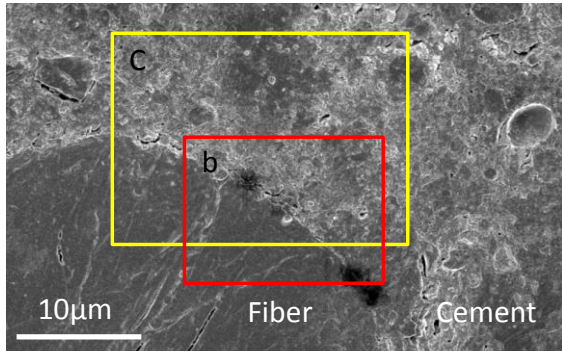
where $\tau_{control}$ is the interface frictional bond strength of specimen without any pre-loading after eight water/air conditioning cycles, which can be derived from the curve of Fig. 4c.

Table 2: Derived interface fractional bond strengths from the fiber pullout force vs. fiber displacement curves

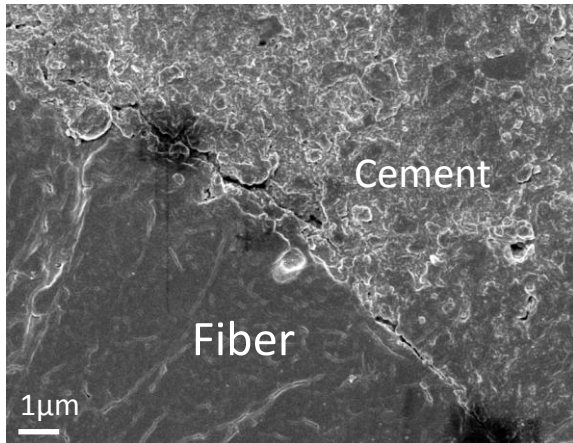
Mix design	Condition regime	Original interface frictional bond, τ_0 (MPa)	Interface frictional bond after healing, τ (MPa)	Healing degree, η (%)
FA0	Air	0.38	0.56 ± 0.27	24
	Water/air	± 0.14	1.49 ± 0.44	63
	Control	-	2.37 ± 0.94	-
FA35	Air	1.41	1.25 ± 0.54	43
	Water/air	± 0.72	2.74 ± 0.55	94
	Control	-	2.91 ± 0.82	-

Table 2 summarizes the interface frictional bond strengths of FA0 and FA35 before and after different conditioning regimes. As can be seen, FA35 has a much higher original interface frictional bond strength τ_0 . Inclusion of fly ash densifies the interface and thus increases the frictional bond strength, which was reported in [13]. Furthermore, FA enhances the healing-induced recovery of interface frictional bond strength. Specifically, the healing degree η increased from 63% to

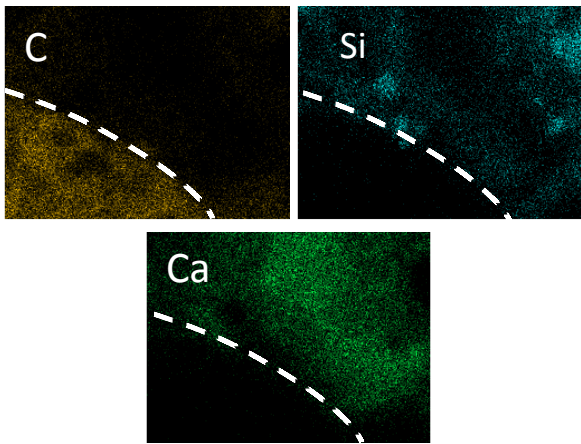
94%, almost complete recovery.



(a)



(b)



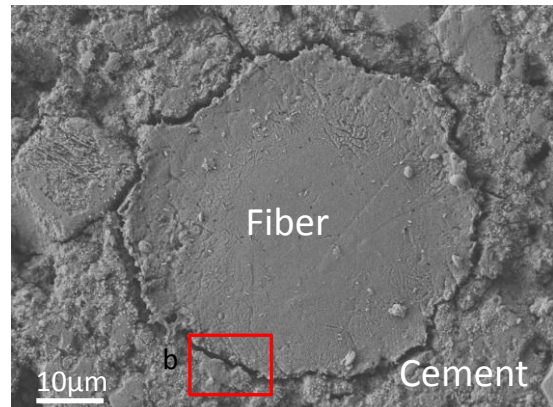
(c)

Figure 5: Original fiber/matrix interface before pre-loading: (a-b) The bonded interface observed with FE-SEM; and (c) the element mapping in the vicinity

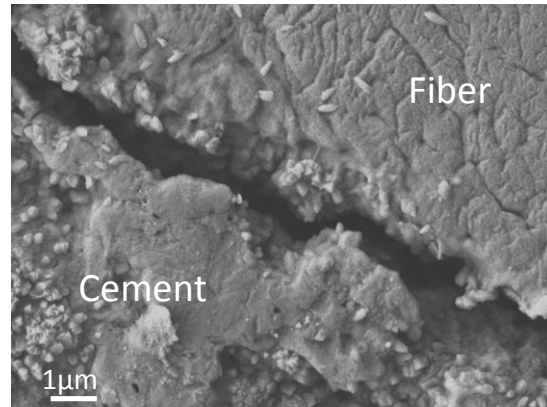
3.3 Microstructures of pre-loaded and healed fiber/matrix interface

Figs. 5 and 6 show the typical microstructure of the fiber/matrix interface

before and after pre-loading, respectively. As can be seen, the original interface (Fig. 5) is intact, which shows a continuous transition from the fiber to the surrounding matrix and no visible gap found in between. The representative element of fiber (Carbon) and cement matrix (Silicon and Calcium), as shown in Fig. 5c, are clearly divided by the boundary. After pre-loading, a ring-shaped interface crack of about 0.5-3 µm wide is observed in Fig. 6a. Distinct surface textures are observed on the different side of the crack (Fig. 6b).



(a)



(b)

Figure 6: Pre-loaded fiber/matrix interface: (a) the ring-shape interface crack between the fiber and cement matrix; (b) the details of the ring crack

Fig. 7 shows the typical microstructure of healed fiber/matrix interface after water/air conditioning (FA35). As can be seen, the interface crack is completely filled with healing products as highlighted by the dash-line envelope in Fig. 7b. The crystal-like

healing products have a dimension of 0.5-2 μm . This shows healing products is able to grow and fill the tight sub-micron interface crack between the fiber and the cement matrix. The elemental mapping is given in Fig. 7c and the quantitative EDX results are presented in Fig. 8. As can be seen, the healing products in the dash-line region is rich in Ca and C but lack of Si. This suggests that the healing products were not C-S-H, which has been reported as one of the major healing products in cement matrix cracks, which are usually much wider (usually $> 10 \mu\text{m}$) than the current interface crack [9, 14]. While both $\text{Ca}(\text{OH})_2$ [15] and CaCO_3 [9, 14] have been reported as the healing products in cement matrix cracks, it is believed CaCO_3 is the major healing product in the current study for the following reasons. Firstly, the morphology of healing products in the current study were stone-like polyhedrons, sharing the same morphology that of calcite found in healed cement matrix cracks, a polymorph of CaCO_3 which has been confirmed by XRD spectroscopy [14]. Portlandite, however, the polymorph found in healed cracks is normally thin plate [15]. Secondly, in the current study, the specimen was exposed to the ambient air during conditioning, where CO_2 was present. It has been reported that $\text{Ca}(\text{OH})_2$ is abundantly present only in the absence of CO_2 [15-16].

3.4 Healing-induced recovery of fiber-bridging strength

Fig. 9 shows the typical reloading curves (fiber-bridging stress vs. extension) of pre-cracked FRCC specimens subject to different conditioning regimens. The fiber-bridging stress is calculated as tensile force divided by the cross sectional area of the dog-bone specimen. As can be seen, pre-cracked FRCC specimens subject to the water/air conditioning shows higher fiber-bridging stiffness and strength than that subject to the air conditioning. As the matrix cracks remains unsealed after conditioning (Table 3), the recovery is mainly attributed to healing of fiber/matrix interface. Furthermore, FA35 FRCC specimens exhibit a much significant

recovery of fiber-bridging stiffness and strength.

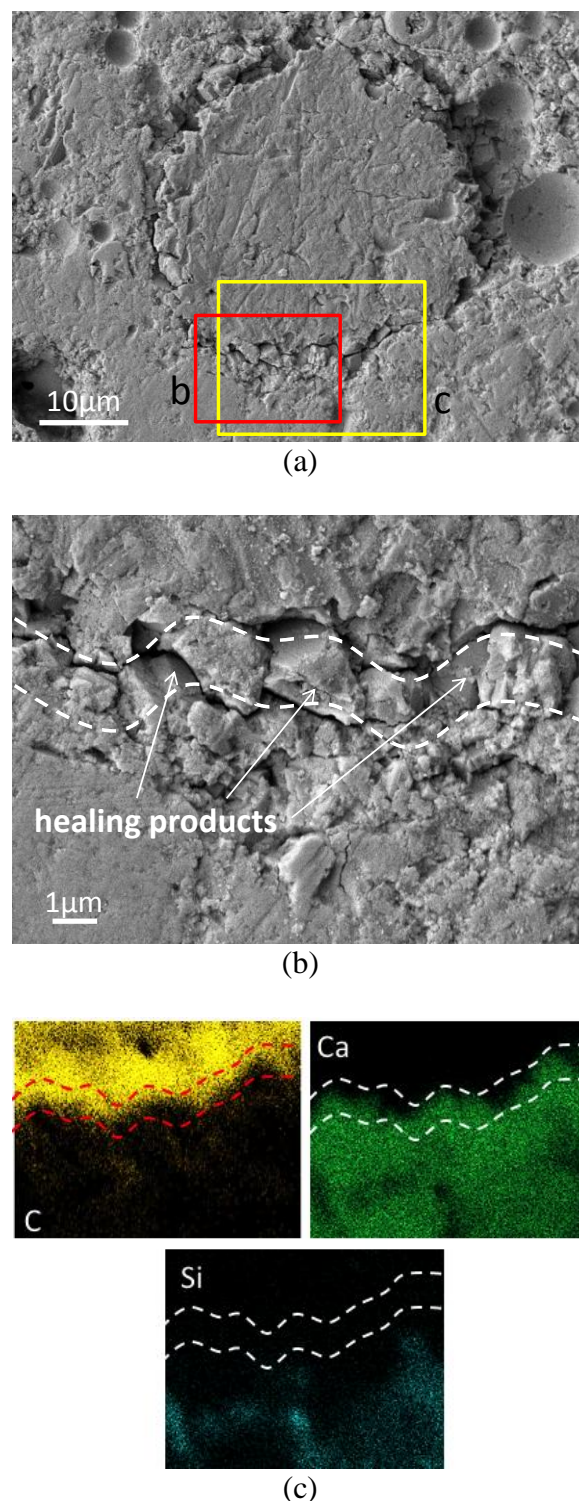
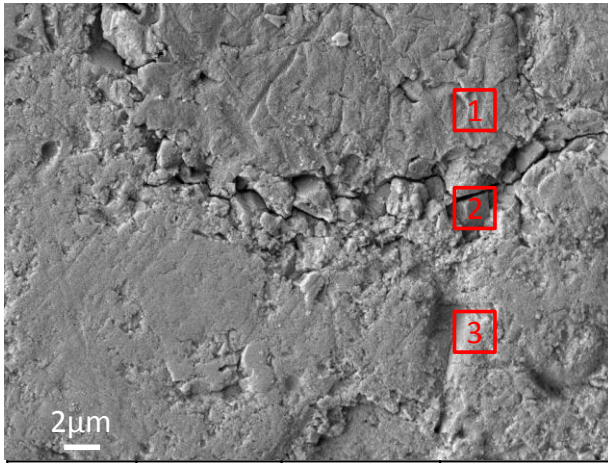


Figure 7: Healed fiber/matrix interface crack after water/air conditioning (FA35): (a-b) The morphology of the healing products observed with FE-SEM; and (c) the elementary composition in the vicinity of the healed crack. The dash lines indicate the location of the interface crack.



Element	Spot 1	Spot 2	Spot 3
C	77.0%	10.6%	11.7%
O	21.5%	50.8%	49.8%
Al	0.0%	0.1%	0.7%
Si	0.0%	0.0%	4.7%
Ca	1.5%	38.1%	31.9%
Others	0.0%	0.4%	1.2%
Ca/Si	N.A.	N.A.	6.8

Figure 8: Quantitative EDX results of the selected spots in the vicinity of the healed fiber/matrix interface.

Table 3 summarizes the crack width of pre-cracked FRCC specimen before and after different conditioning regimes. Fiber-bridging strength of pre-cracked FRCC specimen after different conditioning regimes and healing degree are also reported. The healing degree H is defined as follows,

$$H = \sigma_{\text{reloading}} / \sigma_{\text{control}} \quad (3)$$

where $\sigma_{\text{reloading}}$ is the fiber-bridging strength of pre-cracked FRCC specimen after conditioning (Fig. 9); and σ_{control} is the fiber-bridging strength of FRCC specimen without any pre-cracking after eight water/air conditioning cycles. As can be seen, inclusion of fly ash enhances the healing-induced recovery of fiber-bridging strength. Specifically, the healing degree H increases from 82% to 127%, indicating the healing strategy based on fiber/matrix interface recovery effectively strengthened the fiber-

bridging of FRCC.

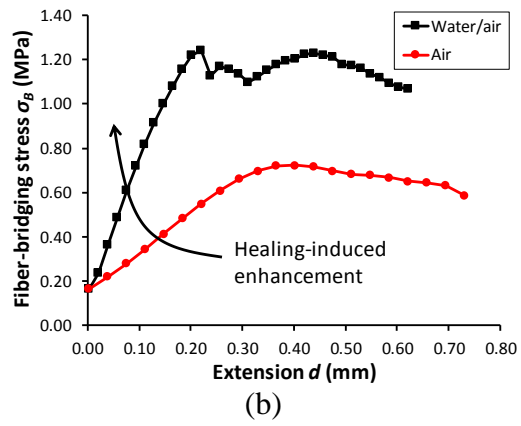
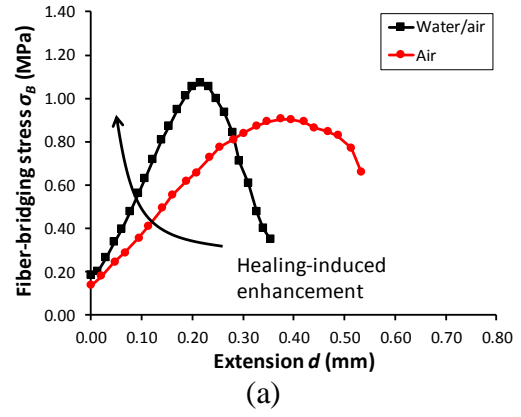


Figure 9: Typical fiber-bridging stress vs. extension (i.e., actuator displacement) curves of (a) FA0 and (b) FA35 subject to different conditioning regimes.

Table 3: FRCC uniaxial tensile test results

Mix	Condition regime	Crack width (μm)		Fiber-bridging strength, σ_c (MPa)	Healing degree, H (%)
		Before healing	After healing		
FA0	Air	70 \pm 24	68 \pm 15	0.98 \pm 0.18	75
	Water/air	68 \pm 38	59 \pm 21	1.07 \pm 0.16	82
	Control	-	-	1.30 \pm 0.15	-
FA35	Air	62 \pm 21	63 \pm 18	0.85 \pm 0.10	89
	Water/air	62 \pm 24	52 \pm 17	1.22 \pm 0.16	127
	Control	-	-	0.96 \pm 0.06	-

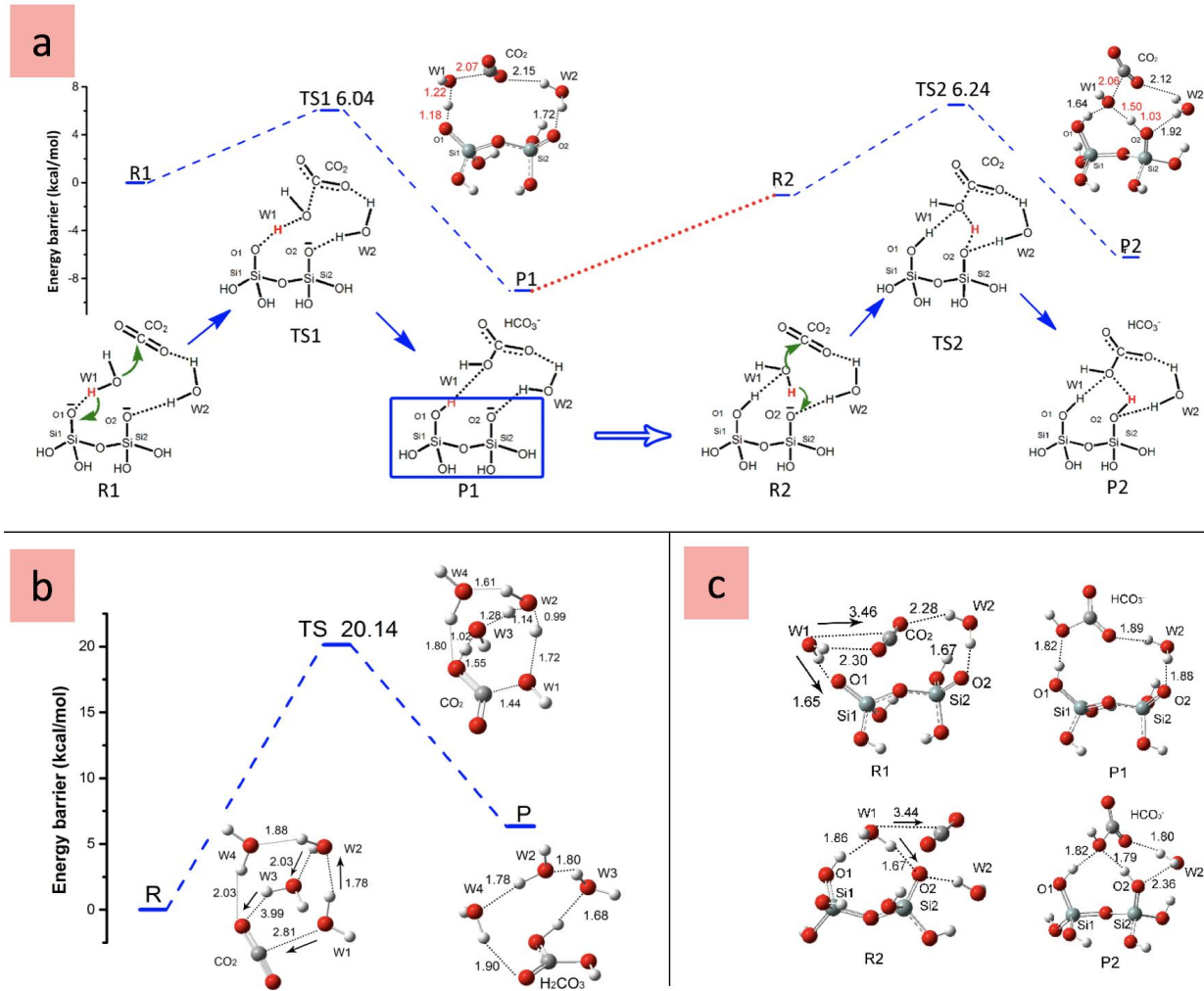


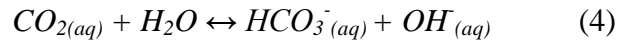
Figure 10: Molecular dynamics simulation: (a) the schematic and the calculated potential energy profiles along the reaction coordinate for HCO_3^- formation on silicate chain. The hydrogen dissociated from the nucleophile water molecule is shown in red. Red dash line represents we just use the product $\text{Si}_2\text{O}_5(\text{OH})_5^-$ as the reactant in the second reaction. Transition states of each reaction are shown. (b) The calculated energy barrier of CO_2 combining H_2O to form H_2CO_3 in the absence of silicate chain. (c) The optimized structures of reactants and products in the proposed mechanisms in (a). Bond length of transition states in Å and energy barriers value in kcal/mol.

3.4 Discussion on the effect of FA on healing products formation

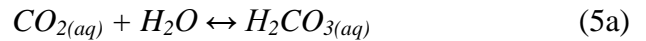
In the current study, it has been shown experimentally that partial replacement of OPC with Class F engaged more healing-induced mechanical recovery at debonded interface between fiber and matrix. Here we tried to discuss the effect of FA on the chemical reactions to form CaCO_3 as healing product by adopting molecular dynamics simulation (MDS).

Chemically, the formation of CaCO_3 in aqueous environment takes the following route

[17-18]:



or



to form bicarbonate, then the deprotonation and CaCO_3 precipitation



Previous experimental and theoretical studies have shown that the formation of bicarbonate HCO_3^- from CO_2 and H_2O is the rate-limiting (Eq. 4 or Eq. 5a) [19-20].

Fig.10a shows the MDS results on the

formation of HCO_3^- in the presence of $\text{Si}_2\text{O}_2(\text{OH})_4^{2-}$, a typical unit structure of silicate chain in cement paste. Two water molecules W1 and W2 are involved and have different functions for this reaction. W1 nucleophilically attacks the CO_2 , as the proton H_{W1} (red) being transferred to the deprotonated O1 in the silicate hydrate $\text{Si}_2\text{O}_3(\text{OH})_4^{2-}$, while W2 anchors the CO_2 molecule. In the transition state TS1, the bond $\text{O}_{\text{W1}}-\text{C}$ is being formed with a bond length 2.07 Å; while the bond $\text{O}_{\text{W1}}-\text{H}_{\text{W1}}$ with the bond length 1.22 Å is breaking. Finally, the HCO_3^- ion is formed. The concerted mechanism is associated with an energy barrier about 6.04 kcal/mol, which is significantly lower than the 20.14-kcal/mol energy barrier seen with during the CO_2 dissolution in solution (Fig. 10b), which is based on the three water-assisted mechanism proposed in [21].

The product $\text{Si}_2\text{O}_2(\text{OH})_5^-$ (P1 or R2 in Fig. 10a) formed in the previous step continues to catalyze the formation of HCO_3^- , which also involves two water molecules W1 and W2, the W1 nucleophilically attacks the CO_2 , as the proton H_{W1} (red) being dragged to O2, the other deprotonated in the silicate chain. In the transition state TS2, the bond $\text{O}_{\text{W1}}-\text{C}$ is being formed with a bond length 2.06 Å; while the bond $\text{O}_{\text{W1}}-\text{H}_{\text{W1}}$ with the bond length 1.50 Å is breaking. The concerted mechanism is associated with an energy barrier about 6.24 kcal/mol, which is still significantly lower than that in conventional CO_2 dissolution in solution. The simulation results indicate that the deprotonation of water by the $\text{Si}-\text{O}^-$ could effectively enhance the chance of HCO_3^- formation and subsequently more CaCO_3 .

Recent study on the molecular structure of C-S-H has shown that C-S-H is made up of layers of dreierkette silicate chains that sandwich an intermediate layer of $-\text{O}-\text{Ca}-\text{O}-\text{Ca}-$ structures [22]. Class F fly ash has significantly richer content of silicate than Portland cement; the partial replacement with FA can greatly reduce the Ca/Si ratio in the C-S-H. In terms of the molecular structures, significant amount of Ca-O groups in the intermediate layers may be replaced, exposing more Si-O- groups to catalyze the reaction for

HCO_3^- formation and subsequently CaCO_3 formation as healing products.

In terms of MDS method, All the calculations were carried out using the M06 functional [23] with the triple- ζ 6-311++G(d,p) basis set in the Gaussian 09 software [24]. Geometry optimizations were done by the Berny algorithm using the standard force and displacement convergence criteria throughout [25]. All the stationary points have been positively identified as minima with no imaginary frequencies and the transitions state as a saddle point on the energy surface with one imaginary frequency. All the calculations that were done using this functional has shown to be adequate for the study of non-covalent interactions, especially hydrogen bonds. For each transition states, the intrinsic reaction coordinate was calculated yielded.

4 CONCLUSIONS

This study examines autogenous healing of interface between micro polymeric fiber and hydraulic cement matrix. Results show that fiber/matrix interface crack the interface frictional bond strength can be significantly recovered while the interface chemical bond can not be re-established after eight cycles of water/air conditioning. The healing products filled in the fiber/matrix interface crack are mainly CaCO_3 which has a crystal-like morphology with a particle size of 0.5-2 μm . Fiber/matrix interface healing results in remarkable recovery of fiber-bridging strength of pre-cracked FRCC. Inclusion of fly ash in the mix composition significantly enhances the autogenous healing of fiber/matrix interface as the healing degree of interface frictional bond strength increases from 63% to 94% and that of the fiber-bridging strength improves from 82% to 127%.

REFERENCES

- [1] Wiktor, V., & Jonkers, H. M. 2011. Quantification of crack-healing in novel bacteria-based self-healing concrete. *Cement Concrete Comp.*, 33(7), 763-770.

- [2] Tziviloglou, E., Wiktor, V., Jonkers, H. M., & Schlangen, E. 2016. Bacteria-based self-healing concrete to increase liquid tightness of cracks. *Constr. Build. Mater.*, 122, 118-125.
- [3] Yang, Z., Hollar, J., He, X., & Shi, X. 2011. A self-healing cementitious composite using oil core/silica gel shell microcapsules. *Cement Concrete Comp.*, 33(4), 506-512.
- [4] Van Tittelboom, K., De Belie, N., Van Loo, D., & Jacobs, P. 2011. Self-healing efficiency of cementitious materials containing tubular capsules filled with healing agent. *Cement Concrete Comp.*, 33(4), 497-505.
- [5] Wu, M., Johannesson, B., & Geiker, M. 2012. A review: Self-healing in cementitious materials and engineered cementitious composite as a self-healing material. *Constr. Build. Mater.*, 28(1), 571-583.
- [6] Edvardsen, C. 1999. Water permeability and autogenous healing of cracks in concrete. *ACI Mater. J.*, 96(4), 448-454.
- [7] Yang, Y., Lepech, M. D., Yang, E. H., & Li, V. C. 2009. Autogenous healing of engineered cementitious composites under wet-dry cycles. *Cement Concrete Res.*, 39(5), 382-390.
- [8] Qian, S., Zhou, J., De Rooij, M. R., Schlangen, E., Ye, G., & Van Breugel, K. 2009. Self-healing behavior of strain hardening cementitious composites incorporating local waste materials. *Cement Concrete Comp.*, 31(9), 613-621.
- [9] Fan, S., & Li, M. 2014. X-ray computed microtomography of three-dimensional microcracks and self-healing in engineered cementitious composites. *Smart Mater. Struct.*, 24(1), 015021.
- [10] Qiu, J., Tan, H. S., & Yang, E. H. 2016. Coupled effects of crack width, slag content, and conditioning alkalinity on autogenous healing of engineered cementitious composites. *Cement Concrete Comp.*, 73, 203-212.
- [11] Qiu, J., Lim, X. N., & Yang, E. H. 2016. Fatigue-induced deterioration of the interface between micro-polyvinyl alcohol (PVA) fiber and cement matrix. *Cement Concrete Res.*, 90, 127-136.
- [12] Redon, C., Li, V. C., Wu, C., Hoshiro, H., Saito, T., & Ogawa, A. 2001. Measuring and modifying interface properties of PVA fibers in ECC matrix. *J. Mater. Civil Eng.*, 13(6), 399-406.
- [13] Wang, S., & Li, V. C. 2007. Engineered cementitious composites with high-volume fly ash. *ACI Mater. J.*, 104(3), 233.
- [14] Kan, L. L., Shi, H. S., Sakulich, A. R., & Li, V. C. 2010. Self-Healing Characterization of Engineered Cementitious Composite Materials. *ACI Mater. J.*, 107(6).
- [15] Huang, H., Ye, G., & Damidot, D. 2013. Characterization and quantification of self-healing behaviors of microcracks due to further hydration in cement paste. *Cement Concrete Res.*, 52, 71-81.
- [16] Palin, D., Wiktor, V., & Jonkers, H. M. 2015. Autogenous healing of marine exposed concrete: characterization and quantification through visual crack closure. *Cement Concrete Res.*, 73, 17-24.
- [17] Wallace, A. F., Hedges, L. O., Fernandez-Martinez, A., Raiteri, P., Gale, J. D., Waychunas, G. A., ... & De Yoreo, J. J. 2013. Microscopic evidence for liquid-liquid separation in supersaturated CaCO₃ solutions. *Science*, 341(6148), 885-889.
- [18] Brečević, L., & Nielsen, A. E. 1989. Solubility of amorphous calcium carbonate. *J. Cryst. Growth*, 98(3), 504-510.
- [19] Dreybrodt, W., Eisenlohr, L., Madry, B., & Ringer, S. 1997. Precipitation kinetics of calcite in the system CaCO₃ · H₂O · CO₂: The conversion to CO₂ by the slow process H⁺ + HCO₃⁻ → CO₂ + H₂O as a rate limiting step. *Geochim. Cosmochim. Ac.*, 61(18), 3897-3904.
- [20] Stirling, A., & Papai, I. 2010. H₂CO₃ Forms via HCO₃⁻ in Water. *J. Phys. Chem. B*, 114(50), 16854-16859.
- [21] Nguyen, M. T., Matus, M. H., Jackson, V. E., Ngan, V. T., Rustad, J. R., & Dixon, D. A. (2008). Mechanism of the hydration

of carbon dioxide: Direct participation of H₂O versus microsolvation. *J. Phys. Chem. A*, 112(41), 10386-10398.

- [22] Richardson, I. G. 2004. Tobermorite/jennite-and tobermorite/calcium hydroxide-based models for the structure of CSH: applicability to hardened pastes of tricalcium silicate, β -dicalcium silicate, Portland cement, and blends of Portland cement with blast-furnace slag, metakaolin, or silica fume. *Cement Concrete Res.*, 34(9), 1733-1777.
- [23] Schaffer, C. L., & Thomson, K. T. (2008). Density functional theory investigation into structure and reactivity of prenucleation silica species. *J. Phys. Chem. C*, 112(33), 12653-12662.
- [24] Zhao, Y., & Truhlar, D. G. 2008. Density functionals with broad applicability in chemistry. *Accounts Chem. Res.*, 41(2), 157-167.
- [25] M.J. Frisch, G. Trucks, H.B. Schlegel, G. Scuseria, M. Robb, J. Cheeseman, G. Scalmani, V. Barone, B. Mennucci, G. Petersson. 2009. *Gaussian 09, revision A.1*, Gaussian Inc.